Reconstruction Algorithm for Sound Speed Distribution in the Female Breast

Omer M. Gaddoura[1], Akram Omara[2], Arkan M. Alromema[1], Suiren Wan[1]

South East University, Nanjing, PRC [1]
Sudan University of Science and Technology, Khartoum, Sudan[2]
omer.bme@gmail.com

Received : 20/7/2019
Accepted : 07/08/2019

ABSTRACT- In the last few years, Ultrasound Computed Tomography (USCT) techniques has become an attractive and hot research area. Herein, we present a robust iterative USCT reconstruction algorithm, which based on bent ray theory. The object to be imaged is encircled by uniformly distributed transducers, whereas one transducer acts as a transmitter and the remains work as receivers. The travel-time measurements can be used to estimate the sound speed distribution by solving a nonlinear system of equations. Our proposed scheme is based on the straight ray approximation, which is valid for breast ultrasound tomographic imaging. On this basis, we have formulated a cost function that defines the difference between the measured first arrivals and those calculated for a given velocity model in the least squares sense. Then, the sound speed image can be obtained by finding the best solution which minimize this difference. Our method is able to resolve very fine details even in very complex structured objects. The presented results approve the accuracy and robustness of our approach for breast screening applications.

Keywords*: Breast Ultrasound; Transmission Tomography; Travel Time Inversion; Iterative Method; Gauss-Newton.*

المستخلص- في السنوات القليلة الماضية ، أصبحت تقنيات التصوير المقطعي بالموجات فوق الصوتية (USCT) منطقة بحث جذابة وساخنة. في هذا البحث نقدم خوارزمية إعادة بناء تكرارية قوية USCT تعتمد علي نظرية الشعاع المنحني. يتم احاطة الجسم المراد تصويره بمحولات موزعة بشكل منتظم، يعمل محول واحد كجهاز إرسال بينما يعمل البقية كمستقبلات. يمكن استخدام قياسات وقت الاستقبال لتقييم توزيع سرعة الصوت عن طريق حل نظام من المعادلات غير الخطية. يعتمد مخططنا المقترح على تقريب الشعاع المستقيم ، وهو صالح للتصوير المقطعي بالموجات فوق الصوتية للثدي. على هذا الأساس ، قمنا بصياغة دالة تكلفة تعرف الفرق بين قياس زمن وصول الأوائل و بين تلك المحسوبة لنموذج سرعة معين بمفهوم المسافه الاصغر. و من ثم يمكن الحصول على صورة سرعة الصوت من خلال إيجاد أفضل الحلول التي تقلل من هذا الفرق. تمتاز طريقتنا هذه بقدرتها علي حل التفاصيل الدقيقة جدًا حتى في الاجسام ذات البنيه المعقدة جدا. النتائج المقدمة تبرهن على دقة وقوة هذه الطريقه في تطبيقات مسح الثدي.

INTRODUCTION

Breast cancer has become one of the most prevalent types of cancers which affecting women. Since 2008, 1.4 million cases have been registered. Half of these cases occurred in the developing countries. In the same year 458,400 deaths occurred due to breast cancer[1]. In 2012, 229,060 (2,190 male, and 226,870 female) new cases have been estimated in US[2]. Numerous studies have proven that the detection of cancer in early stages limits the rate of mortality[3, 4]. Various techniques are in use to detect breast cancer i.e., x-ray mammography, Magnetic Resonance Imaging (MRI), B-Mode Ultrasound etc.

X-ray mammography has a valuable impact in reducing the breast cancer mortality rate, especially in 50-69 years old women. Despite it is effectiveness, mammography has several drawbacks. It has a high rate of false-positive, which leads to additional biopsies and in most of the cases these extra operations show no sign of breast cancers. Having a mammogram subjects the patient to X-rays, which has significant radiation hazards. Besides hazardousness, it requires the breast to be compressed, which it is not comfortable to the patient and more often women avoid mammogram tests. In addition, this compression process for mammography also leads to an inaccurate cancer positioning. To address the mentioned shortcomings of mammography, MRI comes into play[5~7] but it is terrifically expensive and makes its use impractical, especially in the developing countries. On the other hand, conventional B-Mode ultrasound helps in differentiating cysts from the solid mass. How-

ever, it fails to discriminate be- tween benign and malignant tumors. Recently, the use of Ultrasound Computed Tomography (USCT) techniques has become an interesting research area since the work done by Greenleaf et al.[8]. In their state-of-the-art work, it has been demonstrated that using ultrasound transmission tomography to reconstruct physical parameters of the breast (sound speed and attenuation coefficient) can help to distinguish benign from malignant masses. Since then, many studies have been done while exploiting the potential of ultrasound in detection of the breast lesions [9~15].

Image reconstruction methods in USCT can be divided by means of the sound propagation model. Commonly, there are two models in practice, the first one is Wave-based Model, and the other one is derived from the Ray theory. The former model is the most accurate one, since there is no approximation to the wave equation. Hence, in the wave-based USCT, all the effects (diffraction, refraction, scattering, and attenuation etc.) have to be taken into account (without approximation) while the wave is propagating through different me- dia. Due to the actual considerations of various effects, wave-based USCT suffers mainly from two problems. Firstly, solving the full wave equation is impractically expensive and secondly, there exists a demand for huge amount of memory for computational algorithms[16]. To address these problems, a number of re- searchers have considered various approximations and assumptions. Authors in[17, 18] have pointed out the fact that earlier studies have shown that the diffraction effects are not significant when ultrasound waves propagate through the female breast. Therefore, one of the most common assumptions in ultra- sound diffraction tomography is that the scattered field is far smaller than the incident field (Born and Rytov approximations)[19, 20, 21]. Consequently, it has been considered appropriate to make the straight ray approximation (ray-based model) valid for breast ultrasound tomographic technique. In this work, we have developed and investigated a novel technique for solving the inverse problem, which is related to the USCT. As numerous researchers did, we considered the object to be imaged, it is the female breast in this case, is immersed in a water tank, and surrounded by a ring shaped transducer. While one transducer transmitting an ultrasound signal, the remains receive the transmitted, scattered, and reflected signals[22, 23]. Regarding the reconstruction of the USCT image, in the past two decades, various methods have been developed to generate images of the physical parameters of the concerned object. These properties strongly affect the traveling waves through that medium. One of these methods is the travel time tomography. This technique has been used in wide range of applications, especially in geophysics and seismology[24~27]. Basically, travel time tomography involves solving an inverse problem.

The paper outlines are as follows. The first section a brief introduction about ultrasound computed tomography. The theory of our algorithm for sound speed image reconstruction, including the derivation of forward and inverse problems, is presented in the second section. In the third section, numerical results have been discussed. We conclude this study in the fourth section.

Travel Time Tomography

In general, the travel-time tomography attempts to estimate a velocity model from the time of flight measurements that calculated from the received signals. Solution of such problem can be obtained by minimizing the absolute error be- tween the measured data and the simulated data. This process can be modeled as a cost function of the least squares defined between the observed time of flight ($\mathbf{t}^{obs}$) and those calculated for a given velocity model ($\mathbf{t}^{cal}$). Likewise, the travel time tomography can be formulated as solving an inverse problem in the high frequency approximation of ray theory[28]. Principally, the procedure of obtaining a tomographic image of an object from the travel-time data can be accomplished by the following steps:

a) object parameterization;
b) solving the forward (direct) problem;
c) solving the backward (inverse) problem.

Figure 1 describes the relationship between the direct and the inverse problems**.**

Travel Time Computation (Forward problem)

The forward step has been used to estimate the Time of Flight (TOF) between the transmitter and receiver, for a specific sound speed distribution in the media, along certain path. Although, the reflecting boundaries results in a multiple ray paths, we only consider the path with minimum travel-

time because first-arrivals are easier to extract from the ultrasound signal.

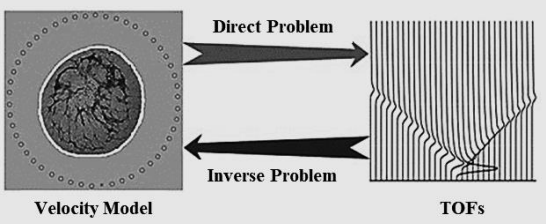

Figure 1: The direct and inverse problems that related to the travel-time tomography, which relates a velocity model to the TOF

The TOF between a source S and a receiver R is related to the speed of sound v(x) by the following equation:

$$t = \int_L s(\mathbf{x})dl \qquad (1)$$

where t is the TOF and the slowness $s(\mathbf{x}) = 1/v(\mathbf{x})$ is the reciprocal of the velocity $v(\mathbf{x})$ .L is the ray path between the source and the receiver. It is assumed that the computational domain has been divided into N number of cells. Here, we considered that each cell exhibits constant sound speed. Mathematically, the discretized version of Equation (1) is given by:

$$t_i = \int_{j=1}^{N} l_{ij}s_j\,;\;\; i = 1,2,3,\cdots,M \qquad (2)$$

where t_i is the TOF between the source S and the receiver R along the path l_{ij} , sj is the slowness at position j, and M is number of transmitter/receiver pairs. In matrix from, the equation appears in (2) can be written as:

$$\mathbf{t} = \mathbf{G}(\mathbf{s}) \cdot \mathbf{s} \qquad (3)$$

where, now, $\mathbf{t}$ is a vector of size $M \times 1$ representing the first arrivals, $\mathbf{s}$ is the slowness of size $N^2 \times 1$, and $\mathbf{G}$ refers to the ray-length matrix of size $M \times N^2$.

The forward problem step is followed by the inverse problem step. The goal of the subsequent step is to find a slowness distribution $\mathbf{s}$ which ultimately used to minimize the cost function.

Travel Time Inversion

In this step, given an accurate set of travel times $t_i(i = 1,2,,M)$ and the estimated distance traveled within each cell, the main objective is to calculate an accurate slowness vector which minimize the following cost function:

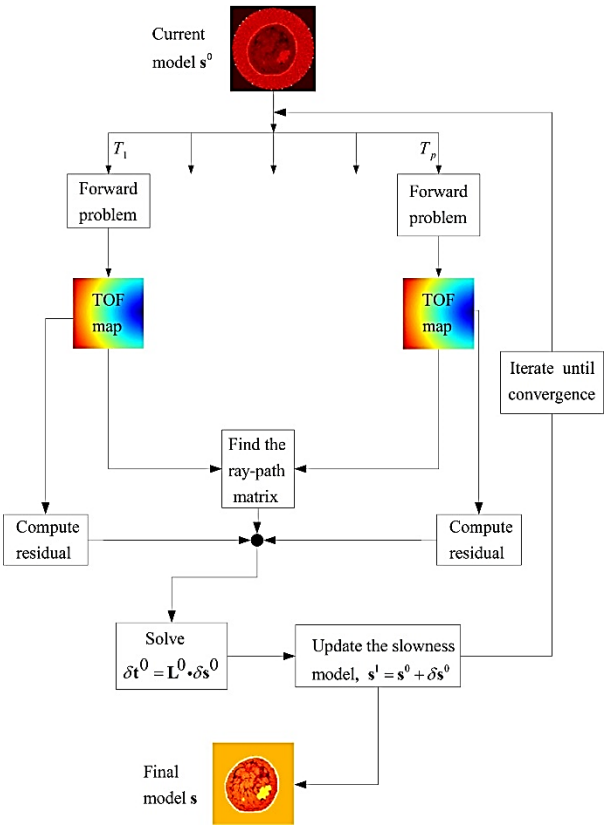

Figure 2: Breast phantom: a) female breast anatomy, b) sound speed phantom of the female breast

$$\mathbf{J}(\boldsymbol{s}) = \frac{1}{2}\sum_{i=1}^{M}\left(\mathbf{t}_i^{cal} - \mathbf{t}_i^{abs}\right)^2 \qquad (4)$$

Our purpose is to minimize $\mathbf{J}(\boldsymbol{s})$. Concerning this, we have exploit the use of the Gauss-Newton (GN) methods. GN starts with an initial guess $\boldsymbol{s}^0$, and iteratively find out the best values for $\mathbf{s}$ that minimize $\mathbf{J}$, as follow

$$\mathbf{s}^{k+1} = \mathbf{s}^k + \delta\mathbf{s}^k \qquad (5)$$

In order to find $\delta\mathbf{s}^k$, we introduced a ray-length matrix $\mathbf{L}_n$ that corresponds to a reference slowness model $\mathbf{s}_n$, which ultimately provides arrival time $\mathbf{t}_n$. For sake of linearization, it is assumed that the real slowness model is equal to

$$\mathbf{s} = \mathbf{s}_n + \delta\mathbf{s}_n \qquad (6)$$

Here, $\delta \mathbf{s}_n$ is a small perturbation with associated travel time $\mathbf{t}$. Fermat's principle states that small perturbation in the slowness does not affect the arrival time[29]. In other words, the ray path remains stationary with small perturbation in the slowness model, as given below

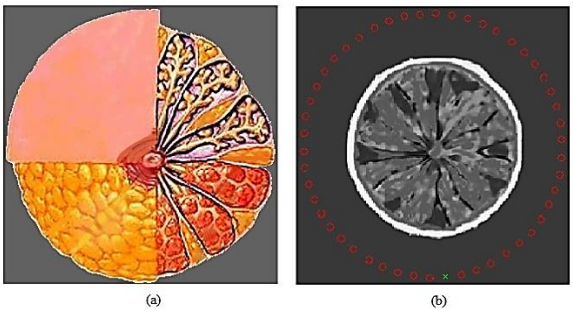

Figure 3: Breast phantom: a) female breast anatomy, b) sound speed phantom of the female breast

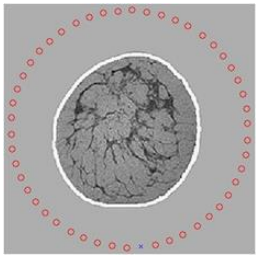

Figure 4: Breast phantom taken from CT scan

$$\mathbf{t} \approx \mathbf{G}_n \cdot \mathbf{s}_n + \mathbf{G}_n \cdot \delta \mathbf{s}_n = \mathbf{t} + \mathbf{G}_n \cdot \delta \mathbf{s}_n \qquad (7)$$

Accordingly, a linearized form can be concluded by setting $\delta \boldsymbol{t}_n = \boldsymbol{t} - \boldsymbol{t}n$ in expression 7. Then, we obtain

$$\delta \mathbf{t}_n = \mathbf{G}_n \cdot \delta \mathbf{s}_n \qquad (8)$$

Then the update step $\delta \mathbf{s}_n$ can be obtained by solving the linear system of equations shown in equation (8). That is to say, the highly nonlinear problem is transformed to a sparse linear system, which can easily be solved by the available numerical methods.

The proposed travel time inversion solution can be summarized in the following steps:

1. set the initial slowness model $\boldsymbol{s}^0$
2. compute the arrival time corresponding to the initial model: $\mathbf{t^0} = \mathbf{G(s)} \cdot \mathbf{s^0}$
3. compute the TOF difference $\delta \mathbf{t}^0 = \mathbf{t}^{obs} - \mathbf{t}^0$
4. calculate the δs0 by solving the linear system: $\delta \mathbf{t^0} = \mathbf{G(s)} \cdot \delta \mathbf{s^0}$
5. update the GN step $\mathbf{s}^1 = \mathbf{s}^0 - \delta \mathbf{s}^0$
6. if $\|\delta \mathbf{t}^0\| \leq \varepsilon_t \ or \ \|\delta \mathbf{s}^0\| \leq \varepsilon_s$ stop. Otherwise, set $\mathbf{s}^1 = \mathbf{s}^0$ and go to step 2

In the proposed algorithm, the most significant point is the step (4), which is related to solving the linear system. It is important to be noted that the number of rays is far greater than the number of cells. This means, the system $\delta \mathbf{t^0} = \mathbf{G(s)} \cdot \delta \mathbf{s^0}$ is an overdetermined. Hence, there is no exact solution, and this becomes a linear least square problem.

B-USCT reconstruction algorithm

The diagram shown in Figure (2) outlines the main algorithmic steps determines the disruption of slowness $\delta \mathbf{s}_n$ for each iteration of the G-NM. From a current model of slowness $\mathbf{s}_n$, solving the direct problem for N shooting points (emitters) provides maps of the first arrival time at all grid points. For all source positions (source/receiver), a path of rays subsequently allows the construction of the Fréchet derivative matrix. This matrix and residuals, calculated from the observed time at the receivers' positions, are then used for iterative solution of linear tomographic system.

RESULTS AND DISCUSSION

Breast phantoms: To test our reconstruction algorithm, we have used two computer generated phantoms. The first one is taken from a female breast photograph. Figure (3-a) shows a female breast anatomy and Figure (3-b) shows sound speed phantom of the female breast.

TABLE 1: SOUND SPEED DISTRIBUTION IN THE FEMALE BREAST

Tissues Type	Speed of sound [m/s]
Water	1500
Lobules	1450-1475
Fatty tissues	1375-1400
Lesions	1530-1560
Skin	1600

The second phantom is more realistic as shown in Figure (4), which was designed from a Computer Tomography (CT) image[30]. Next, we have mapped the CT scan image to the corresponding sound speed distribution. The distributions for the different breast tissues have been given in Table (1). The red circles in Figure (3) and Figure (4) represent the receivers positions, and the cross symbol (×) illustrates the emitter's position.

As already has been discussed in the previous section, the most important step in our algorithm is step (4), where the system of linear equations have to be solved. It should be noted that the ray-path matrix **G** is a very large and sparse. In this work, we have assessed several methods for solving large sparse systems. Explicitly, Bi-Conjugate Gradients (BCG), Stabilized Bi-Conjugate Gradients (SBCG), Quasi-Minimal Residual (QMR), Generalized Minimum Residual (GMR), Least Squares (LSQR), Minimum residual (MR), Preconditioned Conjugate Gradients (PCG), Symmetric LQ

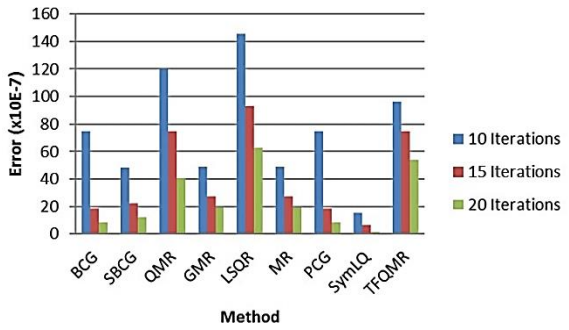

Figure 5: Number of iterations vs. errors

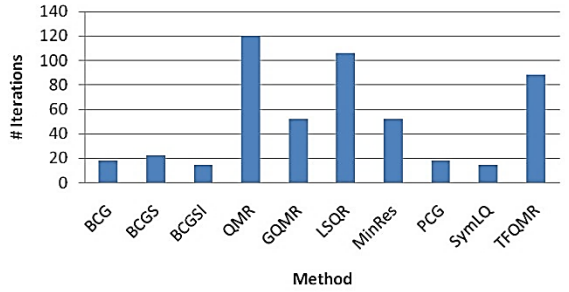

Figure 6: The number of iterations when we used each of the above methods

(SymLQ), and Transpose-free quasi-minimal residual (TFQMR). To test the impact of each method to our algorithm convergence, we have used the phantom shown in Figure (3) of size 128x128, with 150 emitters and 150 receivers. At the first step, we have fixed the number of iterations (10, 15, and 20).

In Figure (5), the error represents the difference between the real (measured) data and calculated (simulated) data. It becomes evident from this figure that SymLQ shows better results in terms of error at all number of iterations. On the other hand, although LSQR with higher error rate shows low performance at all number of iterations, it is observed that LSQR is much faster than other.

Figure (6) shows the number of iterations that our algorithm takes to achieve the desired error, which is equal to 1×10^{-6}. Results displayed in this figure demonstrates that for a fixed error rate the SymLQ method used lower number of iterations.

TABLE 2: THE EFFECT OF CHANGING THE NUMBER OF RECEIVERS

number of Receivers	Error	number of iterations	Elapsed time (s)
50	9.96E-07	44	1
100	9.59E-07	91	4
150	9.07E-07	90	5
200	9.75E-07	83	6
250	8.17E-07	117	11

TABLE 3: THE EFFECT OF CHANGING THE NUMBER OF TRANSMITTERS

number of Transmit-	Error	number of itera-	Elapsed time (s)
50	9.98E-07	56	2
100	9.64E-07	69	3
150	9.97E-07	86	5
200	9.93E-07	98	7
250	8.17E-07	117	11

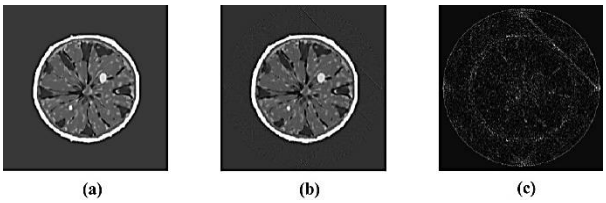

Figure 7: The absolute error for phantom 1: a) The original breast phantom of size 256x256. b) The travel time reconstruction. c) The absolute difference

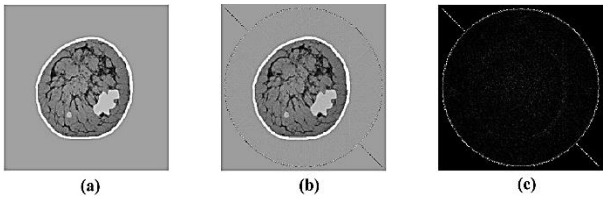

Figure 8: The absolute error for phantom 2: a) The original breast phantom of size 256x256. b) The travel time reconstruction. c) The absolute difference

Also we have measured the reconstruction time of this technique, it is found that the LSQR is fast and effective in terms of time consumption and computational complexity. Although it needs more

number of iterations, it takes less than two seconds to reconstruct a 128 × 128 image.

The number of transmitters and receivers also is a significant factor. In order to investigate the effect of changing the number of transmitters and receivers, we used the phantom shown in Figure (4) of different sizes (128×128, 256×256, and 512×512), with number of transmitters\receivers ranging from 50 to 250. Tables 2 and 3 show the obtained results when the image size is (256×256). We have found that the acceptable number of transmitters\receivers

TABLE 4: QUALITY MEASUREMENT PARAMETERS FOR THE TWO PHANTOMS APPEAR IN FIG.7 AND FIGURE (8)

Phantom/ QMP	MSE	PSNR	CC	SSIM
Phantom (1)	5.757	40.5311	0.9922	0.8531
Phantom (2)	11.7847	37.4176	0.9746	0.8317

depends on the required resolution. Typically, the best option of the number of transmitters and receivers is equal to the required resolution. In other words, if the desired resolution of the reconstructed image is 256×256 pixels, we should use 256 transducers.

It is interesting to compare the reconstructed images with respect to the original speed distribution. As an assessment to the results obtained by our algorithm we define the following quality measurements parameters (QMP):

- Absolute Relative Error (ARE): defined as:

$$\frac{SS_{org} - SS_{rec}}{SS_{org}}$$

- Mean Square Error (MSE): is the measure of average squared difference between the original sound speed SS_{org} and the reconstructed sound speed SS_{rec} It is defined as:

$$MSE = \frac{1}{N}\sum_{i=1}^{N}\left[SS_{org}(i) - SS_{rec}(i)\right]^2$$

- Peak Signal to Noise Ratio (PSNR) : is the measure of the beak error, it defines the ratio between the maximum value of SS_{org} and the MSE

$$PSNR = 10\log\left[\max\left(\frac{SS_{\text{org}}}{MSE}\right)\right]$$

- Correlation Coefficient (CC): measure the similarity between SS_{org} and SS_{rec}

$$CC = \frac{(SS_{\text{org}} - \mu_{org})(SS_{\text{rec}} - \mu_{rec})}{\sqrt{(SS_{\text{org}} - \mu_{org})^2 (SS_{\text{rec}} - \mu_{rec})^2}}$$

- Structural Similarity Index (SSI): measure the similarity structure[31], SSI can be defined as:

$$SSI = \frac{[2\mu_x\,\mu_y + C_1][2\sigma_{xy} + C_2]}{[\mu_x^2 + \mu_y^2 + C_1][\sigma_x^2 + \sigma_y^2 + C_2]}$$

Where

μ_x and μ_y are the means of the original and reconstructed images respectively.

σ_x^2 and σ_y^2 are the variance of the original and reconstructed images respectively.

σ_{xy} is the covariance.

$C_1 = (k_1 L)^2$, and $C_2 = (k_2 L)^2$

in this paper we took $k_1 = 0.01$, $k_1 = 0.03$, and L is the dynamic range of the pixel values.

Furthermore, we have analyzed the quality of the reconstructed image by calculating the absolute error, i.e. the absolute difference between the breast phantom and its reconstructed image. For illustration purposes, Figures (7) and (8) show the obtained results, we have noticed that with the same number of pixels, and number of transmitters receivers, the error is larger for the high-contrast media. However, the image quality can be improved by increasing the number iterations.

CONCLUSIONS

We have implemented the travel time tomography, which applicable under certain conditions. Previous studies have pointed out that the diffraction effects are not significant when ultrasound waves propagate through the female breast. Therefore, these approaches exploited the straight ray approximation, which is valid for breast ultrasound tomographic imaging. We have formulated the problem of the tomographic breast imaging by constructing a cost function. This function defines the difference between the observed first arrivals, and those calculated for a given velocity model in the least squares sense. Then, we have employed G-NM iterative scheme to minimize this function. We have proposed a robust iterative scheme for B-USCT. Each iteration of the proposed method involves solving a large linear system. Accordingly, we have tested different available method for soling large sparse system of equations. The numerical results showed that SymLQ method gives better results (minimum error). Although LSQR with higher error rate shows low performance, it is observed that LSQR is much faster than other meth-

ods. Finally, many quality parameters can been estimated, which show that this approach is superior to the DT and wave-bast tomography.

REFERENCES

[1] W. H. Organization, , 2010, World health statistics 2010, World Health Organiza- tion.

[2] L. A. Torre, F. Bray, R. L. Siegel, J. Ferlay, J. Lortet-Tieulent, A. Jemal, (2015) , Global cancer statistics, 2012, CA: a cancer journal for clinicians 65 (2), 87–108

[3] B. H. Drukker, (1996) , Breast disease: a primer on diagnosis and management., International journal of fertility and women's medicine 42 (5), 278–287.

[4] P. Pisani, D., (2004), Forman, Declining mortality from breast cancer in yorkshire, 1983–1998: extent and causes, British journal of cancer 90 (3), 652–656.

[5] I. Jatoi, (2004), Mri in breast cancer management: potential for benefit and harm., International journal of fertility and women's medicine 50 (6), 281–284.

[6] L. Turnbull, S. Brown, I. Harvey, C. Olivier, P. Drew, V. Napp, A. Hanby, J. Brown, (2010), Comparative effectiveness of mri in breast cancer (comice) trial: a randomised controlled trial, The Lancet 375 (9714), 563–571.

[7] C. D. Lehman, M. D. Schnall, (2005), Imaging in breast cancer: magnetic resonance imaging, Breast Cancer Research 7 (5), 215.

[8] J. F. Greenleaf, S. Johnson, R. C. Bahn, (1977), Quantitative cross-sectional imag- ing of ultrasound parameters, in: Ultrasonics Symposium, IEEE, 1977, pp. 989–995.

[9] P. L. Carson, C. R. Meyer, A. L. Scherzinger, T. V. Oughton, (1981), Breast imag- ing in coronal planes with simultaneous pulse echo and transmission ultra- sound, Science 214 (4525), 1141–1143.

[10] S. A. Johnson, M. L. Tracy, (1983), Inverse scattering solutions by a sing basis, multiple source, moment methodpart i: Theory, Ultrasonic Imaging 5 (4), 361–375.

[11] M. P. Andr´e, H. S. Jan´ee, P. J. Martin, G. P. Otto, B. A. Spivey, D. A. Palmer, (1997) , High-speed data acquisition in a diffraction tomography system employing large-scale toroidal arrays, International Journal of Imaging Sys- tems and Technology 8 (1), 137–147.

[12] D.-L. Liu, R. C. Waag, (1997), Propagation and backpropagation for ultrasonic wavefront design, IEEE transactions on ultrasonics, ferroelectrics, and fre- quency control 44 (1), 1–13.

[13] S. A. Johnson, D. T. Borup, J. W. Wiskin, F. Natterer, F. Wubeling, Y. Zhang, S. C. Olsen, (1999), Apparatus and method for imaging with wavefields using inverse scattering techniques, uS Patent 6,005,916.

[14] V. Z. Marmarelis, T.-S. Kim, R. E. Shehada, (2003), High-resolution ultrasound transmission tomography, in: Medical Imaging 2003, International Society for Optics and Photonics, pp. 33–40.

[15] N. Duric, P. Littrup, L. Poulo, A. Babkin, R. Pevzner, E. Holsapple, O. Rama, C. Glide, (2007), Detection of breast cancer with ultrasound tomog- raphy: First results with the computed ultrasound risk evaluation (cure) prototype, Medical physics 34 (2), 773–785.

[16] O. M. Gaddoura, W. Longhui, D. Mingyue, H. Jinchun (2011), Breast ultrasound tomography using homotopy continuation method, in: Intelligent Compu- tation and Bio-Medical Instrumentation (ICBMI), 2011 International Con- ference on, IEEE, pp. 4–7.

[17] Q. Zhu, B. D. Steinberg, (1994), Wavefront amplitude distribution in the female breast, The Journal of the Acoustical Society of America 96 (1), 1–9.

[18] S. Li, M. Jackowski, D. P. Dione, T. Varslot, L. H. Staib, K. Mueller, (2010), Re- fraction corrected transmission ultrasound computed tomography for ap- plication in breast imaging, Medical physics 37 (5), 2233–2246.

[19] M. M. Bronstein, A. M. Bronstein, M. Zibulevsky, H. Azhari, (2002), Recon- struction in diffraction ultrasound tomography using nonuniform fft, IEEE transactions on medical imaging 21 (11), 1395–1401.

[20] D. H. Chambers, P. J. Littrup, (2002), Ultrasound imaging using diffraction tomog- raphy in a cylindrical geometry, in: Medical Imaging 2002, International Society for Optics and Photonics, pp. 412–420.

[21] O. M. Gaddoura, M. Ding, (2011), Diffraction tomography: It's application in ul- trasound, International Journal of Engineering and Manufacturing (IJEM) 1 (4) ,10.

[22] R. C. Waag, R. J. Fedewa, (2006), A ring transducer system for medical, IEEE transactions on ultrasonics, ferroelectrics, and frequency control 53 (10).

[23] R. Stotzka, J. Wuerfel, T. O. Mueller, H. Gemmeke, (2002) Medical imaging by ultrasound computer tomography, in: Medical Imaging 2002, International Society for Optics and Photonics, pp. 110–119.

[24] J. G. Berryman, (1993), Global extrema in traveltime tomography, Computational Acoustics 2, 45–62.

[25] J.-W. Huang, G. Bellefleur, (2012) Joint transmission and reflection traveltime to- mography using the fast sweeping method and the adjoint-state technique, Geophysical Journal International 188 (2), 570–582.

[26] N. Rawlinson, M. Sambridge, (2003), Seismic traveltime tomography of the crust and lithosphere, Advances in Geophysics 46, 81–199.

[27] C. Taillandier, M. Noble, H. Chauris, H. Calandra, (2009) First-arrival traveltime tomography based on the adjoint-state method, Geophysics 74 (6), WCB1–WCB10.

[28] A. Tarantola, A. Tarantola, (1987) Inverse problem theory, vol. 130.

[29] J Gance, G Grandjean, K Samyn, JP Malet, (2012), Quasi-Newton inversion of seismic first arrivals using source finite bandwidth assumption: Application to subsurface characterization of landslides, Journal of Applied Geophysics.

[30] J. M. Boone, A. L. Kwan, K. Yang, G. W. Burkett, K. K. Lindfors, T. R. Nelson, (2006), Computed tomography for imaging the breast, Journal of mammary gland biology and neoplasia 11 (2) 103–111.

[31] Z. Wang, A. C. Bovik, H. R. Sheikh, E. P. Simoncelli, (2004), Image quality assessment: from error visibility to structural similarity, IEEE transactions on image processing 13 (4), 600–612.